Trends in Social Sciences and Humanities Research
ISSN: 2959-9938
DOI: https://doi.org/10.61784/tsshr3132

THE PROBLEM OF BENCH DRAGON ENTERING AND EXITING THE SPIRAL MOTION WITH CONSTANT DISTANCE

YiHeng Zhang
School of Mathematics and Statistics, Beijing Jiaotong University, Beijing 100044, China.
Corresponding Email: 22271080@bjtu.edu.cn

Abstract: With the acceleration of China's socialist modernization process, the protection and innovation of traditional folk culture have become the focus of societal attention. This paper focuses on the unique folk activity of the Bench Dragon, which is found in regions such as Zhejiang and Fujian. It conducts an in-depth study of the problem of the Bench Dragon entering and exiting the spiral motion with constant distance, aiming to provide theoretical support for the inheritance and development of this traditional folk custom. Through the analysis of the Bench Dragon's motion trajectory, speed variation, collision conditions, and turning areas, this paper establishes a mathematical model for the Bench Dragon's equidistant spiral motion. The model utilizes recursive formulas, geometric relationships, trigonometric theorems, and the simulated annealing algorithm to thoroughly explore the motion laws during the entering and exiting process. The study finds that there are collision risks during the entering and exiting process, calculates the time point of the first collision, and determines the minimum pitch that satisfies the turning conditions. Additionally, the paper analyzes the impact of the dragon head's speed variation on the dragon body's speed and derives the limiting speed of the dragon head. The research results show that the model and methods established in this paper can effectively guide the arrangement and safety of Bench Dragon performances, which is of significant importance for promoting the inheritance and innovation of traditional folk culture.
Keywords: Equidistant spiral motion; Simulated annealing algorithm; Bench dragon

1 INTRODUCTION

With the gradual advancement of Chinese-style modernization, the country has increasingly emphasized the integration of excellent traditional Chinese culture with modern technology, promoting the innovation and development of traditional folk culture. In particular, traditional local folk activities in regions like Zhejiang and Fujian continue to maintain vibrant vitality. The "Bench Dragon," as one of the region's unique folk cultural activities, has become an important festive event for local people due to its distinctive form of expression. The dragon dance involves connecting multiple segments of benches with the dragon's head leading, and the entire dragon team performs smooth movements along specific trajectories through continuous entering and exiting, showcasing strong local characteristics and the charm of folk art. This paper, addressing research issues related to this traditional folk activity, will establish a mathematical model based on equidistant spiral motion, focusing on the dynamic process of 1 dragon head and 223 dragon body segments during the entering and exiting process.

Currently, scholars both domestically and internationally have conducted research on equidistant spiral motion. Zhoulin Ding and Yongji Yu derived the Archimedean spiral equation describing the spiral intensity pattern by analyzing the propagation dynamics of AS beams and demonstrated that the intensity distribution of AS beams follows an equidistant spiral [1]. Weishuai Cui and others developed a collision detection model based on spiral geometric properties and used particle swarm optimization (PSO) and feedforward neural networks to determine the minimum pitch angle [2]. David Eppstein proved that every star-shaped or spiral-shaped domain in three-dimensional Euclidean space is unlockable and can be unfolded into a planar embedding through a continuous motion [3]. Lei Yang and others used discrete element methods and physical experiments to simulate and test the mass flow, material density [4], and dust concentration of equidistant spiral and non-axial (variable pitch) spiral conveying environments, obtaining a maximum dust elevation of 37.88%. Jhon Jasper D. Apan and others used computational fluid dynamics (CFD) to determine how the matching angle influences the hemodynamics of spiral flow-induced plant designs [5]. Shuangqing Yu and others established a kinematic model for equiangular spiral folding patterns based on the kinematic equivalence of rigid origami and spherical linkages [6]. Wenjian CAO and others proved the trajectory of the cathode tool center satisfies the Archimedes spiral equation, and the feed depth in adjacent cycles is a constant [7]. Greco C and others proposed a scalable automated manufacturing system for the efficient production of twisted spiral artificial muscles (TSAM) [8], reducing manufacturing time by 75% and achieving high automation of servo motors. Hai Zhu and others achieved low disturbance on the cutting surface of hydrate samples by studying the Archimedean spiral [9], providing precise control over the process. Peterman DJ and others studied the fluid statics and fluid dynamics of spiral-shaped corn cones through virtual modeling [10], computational fluid dynamics simulation, and water chamber experiments, using Cenomanian (Cretaceous) turrilitid Mariella-brazoensis (Roemer, 1852) as a test case. Ping Liu and others analyzed the characteristics of the Archimedean spiral equation [11], calculated interpolation points using the angle as a variable and the equiangular straight-line approximation algorithm. Katherine Longardner and others proposed a new algorithm to measure the amplitude of tremor movement using digital equidistant spiral diagrams and established its reliability and clinical practicality through the V3 framework (sensor validation, analysis validation, and clinical validation) [12].

2 THE BASIC FUNAMENTAL OF BP NEURAL NETWORK

2.1 Description of the Bench Dragon Motion Model

2.1.1 Equidistant spiral motion curve

In the polar coordinate system, any segment of the dragon dance team entering the spiral motion satisfies the equation of the equidistant spiral curve, which can be expressed as:

$$r(\theta) = r_0 + \frac{p}{2\pi}\theta \tag{1}$$

In this context, r(θ) represents the radial distance corresponding to the angle θ; r0 is the initial radial distance at the starting point, which in this scenario is set to 0, corresponding to an angle of 32π; p is the pitch, which is set as a constant value of 0.55 meters in the equidistant spiral motion; θ(t) is the angular position, which gradually decreases over time.

2.1.2 Motion path of the dragon head

During the spiral motion, this paper define the linear velocity of the dragon head as a constant v=1 m/s, and the infinitesimal line element ds along the spiral can be expressed as:

$$ds = \sqrt{dr^2 + (rd\theta)^2} \tag{2}$$

Based on the spiral equation in equation (1), this paper take the differential of both sides, resulting in $dr = \frac{p}{2\pi}d\theta$. Therefore, equation (2) can be simplified as:

$$ds = \sqrt{(\frac{p}{2\pi}d\theta)^2 + \left((r_0 + \frac{p}{2\pi}\theta)d\theta\right)^2} \tag{3}$$

Thus, this paper have initially established the differential equation expression with respect to θ\thetaθ. Next, this paper will simplify it further based on the given conditions.

2.1.3 The relationship between velocity and the angular change

Since the linear velocity of the dragon head is constant at v=1 m/s, this paper can substitute this into (3). Combining this with the above equation, this paper obtain the differential equation expression for the front handle of the dragon head at any given moment. To simplify further, this paper can proceed as follows:

$$\frac{d\theta}{dt} = \frac{1}{\sqrt{(\frac{p}{2\pi})^2 + \left(r_0 + \frac{p}{2\pi}\theta\right)^2}} \tag{4}$$

This equation indicates that the rate of change of the polar angle θ is related to the radius r(θ) and the pitch p. To obtain the expression for θ(t), this paper can integrate the above equation:

$$t = \int_0^{\theta(t)} -\frac{d\theta}{\sqrt{(\frac{p}{2\pi})^2 + \left(r_0 + \frac{p}{2\pi}\theta\right)^2}} \tag{5}$$

2.1.4 Further determination of the position of the front handle of bench dragon

It is not difficult to deduce that when the position of the front handle of the dragon head is determined at a fixed moment, the positions of the remaining body and tail segments are also determined. For any two adjacent segments, this paper can derive a recursive formula similar to the one in the lemma by following the same relationship.

$$d^2 = r_{i-1}(t)^2 + r_i(t)^2 - 2r_0(t)r_i(t)\cos\left(\theta_{i-1}(t) - \theta_i(t)\right), i = 1, 2...223 \tag{6}$$

$$r_i(t) = r_{i-1}(t) + \frac{p}{2\pi}(\theta_i - \theta_{i-1}), i = 1, 2...223 \tag{7}$$

For the nonlinear system, this paper need the maximum non-unique solutions. This paper set the initial guess by slightly increasing the radial distance of the last point plus bench length to ensure the solution matches the next point's front handle in the spiral-in.

After obtaining the position coordinates of the front handles of each segment and the rear handle of the dragon's tail in the polar coordinate system for the time interval from 0 to 300 seconds, this paper convert the polar coordinates to Cartesian coordinates by following the same steps as before, yielding the position coordinates in the Cartesian coordinate system as follows:

$$x = r\cos\theta \tag{8}$$

$$y = r\sin\theta \tag{9}$$

2.2 Analysis of Collision Conditions in the Bench Dragon Movement

As the Bench Dragon spirals inward, the distance between benches decreases, risking collision. This paper must identify the first collision point and handle positions. Using the law of sines, the dragon head, with its longer side, will be the first to collide due to its leading position and decreasing radial distance. As the spiral tightens, the head reaches a smaller radius first and, with constant velocity, quickly runs out of space, stopping the movement before the body and tail, which still have room to maneuver. As a result, the dragon head is the first to experience a collision due to lack of space. The specific collision constraints are as follows:

(1) Velocity condition: The velocity after the collision is zero.

(2) Overlap condition: The benches can overlap at the edges, but the benches and handles must not overlap or collide. Normally, the line connecting the center of the front handle and the outermost point of the front side of the bench is not collinear with the radial distance of the front handle. However, this paper considers the extreme case where the outermost point on the front side of the bench coincides with the outer spiral. In this case, a collision may occur. As shown in the diagram below, when the bottom right vertex E of the dragon head touches the handle on the outer spiral, the radial distance OB and the pitch BE are aligned, and the points OA, AE, and OE form a triangle. In this case, the collision condition is:

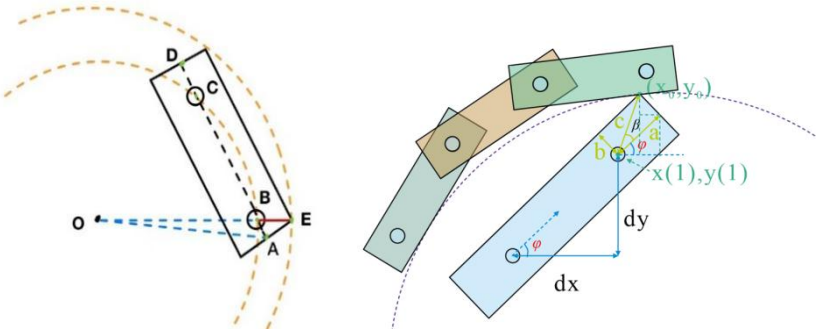

Figure 1 Collision Local Analysis Diagram

Assuming the coordinates of the front and rear handles of the dragon head are (x1,y1) and (x2,y2), this paper now derive the vertex where the dragon head collides in the extreme case, based on the geometric relationships and trigonometric equations, such as the Cartesian coordinates (x0,y0) of the top-right endpoint of the dragon head, as shown in Figure 1.

$$dx = x_2 - x_1 \tag{10}$$

$$dz = \sqrt{(dx)^2 + (y_2 - y_1)^2} \tag{11}$$

$$\varphi = \arccos\frac{dx}{dz} \tag{12}$$

Using the right-angle relationship shown in Figure 1, this paper can derive:

$$\beta = \arccos\frac{a}{\sqrt{a^2 + b^2}} \tag{13}$$

$$x_0 = x_1 + c \cdot \cos(\varphi + \beta) \tag{14}$$

$$y_0 = y_1 + c \cdot \sin(\varphi + \beta) \tag{15}$$

The distance z0 from the collision point to the center can be calculated in the extreme case:

$$z_0 = \sqrt{x_0^2 + y_0^2} \tag{16}$$

Based on the geometric relationships in the extreme case, this paper can derive:

$$z \approx \rho_1 + 55 - 30 \tag{17}$$

$$0 < \rho_1 + 55 - 30 < 0.01 \tag{18}$$

At this point, the dragon head continuously approaches, causing the pitch of the outer spiral to converge with the radial distance of the vertex.

2.3 Analysis of the Bench Dragon Turnaround Area

In the case where the pitch is uncertain and the velocity of the dragon head's front handle is 1 m/s, after the Bench Dragon has moved into a certain position along the spiral, a turnaround is required. This paper define the turnaround area as a circle with a diameter of 9 meters, and based on this, this paper calculate the minimum pitch at which the Bench Dragon can reach the boundary of the turnaround space.

Similar to the analysis in section 2.2, the risk of collision increases as the Bench Dragon moves gradually towards the center of the spiral, and this risk also increases as the pitch decreases. Therefore, this paper must ensure that no collision occurs before the front handle reaches the turnaround area. That is, this paper need to find the pitch at which the collision occurs exactly at the boundary of the turnaround area. This pitch is the minimum pitch that satisfies the required conditions. From the above analysis, this paper can see that the constraint conditions have changed. The new constraints are as follows:

(1) The velocity of the dragon head's front handle is constant at 1 m/s.

(2) The bench is a rigid body, and the distance between adjacent handles is fixed.

(3) The front handle of the dragon head must be able to move along the corresponding spiral path to reach the boundary of the turnaround area with a diameter of 9 meters.

Using the conclusions derived in section 2.2, this paper need to find the smallest pitch d that satisfies the above three constraints. To determine the minimum pitch under the most extreme conditions, this paper strengthen constraint 3 to "The dragon head must exactly collide when it reaches the boundary of the 9-meter diameter turnaround area (the dragon dance team can no longer continue moving inwards)." At this point, the pitch takes its boundary value, and the resulting pitch is the minimum pitch.

To avoid collisions between the benches outside the turnaround area, this paper must ensure that the pitch is greater than a minimum value, with no upper limit. The minimum pitch that satisfies the conditions is the final result that the algorithm aims to obtain. To improve algorithm efficiency, this paper have pre-defined the range of possible values for the minimum pitch based on multiple experimental and computational results.

2.4 Bench Dragon Turnaround Path Analysis

This paper adjust the pitch to 1.7m and maintain the dragon head’s front handle velocity at 1 m/s. The Bench Dragon’s turnaround path within a defined area consists of two S-shaped, tangent semicircles with the first arc twice the radius of the second. This paper design the shortest circular arc path tangent to the inward and outward spirals. A motion model for the “inward → turnaround → outward” sequence is created, solving for handle positions and velocities. The turnaround arcs are tangent to both spirals, making the outward spiral a 180° rotation of the inward spiral. The pitch at the arc boundaries is consistent, and the outward spiral lies between inward spiral arms. With a pitch of 1.7m and each bench covering a max of 32.32cm, no collisions occur between inward and outward spiral benches.

Based on the above analysis and section 2.3 settings, this paper calculate the position and velocity of the dragon head during the turnaround process using the method outlined in section 2.1. Using the recursive formula, this paper further calculate the positions and velocities of the dragon body during the turnaround process and record the results. Since the angles of the two arc sections are unknown, this paper set the angle of the longer arc as a variable. To solve for the shortest curve, this paper convert this into an optimization problem and solve it using an improved simulated annealing algorithm.

Simulated Annealing (SA) is a stochastic optimization algorithm mainly used to find approximate global optimum solutions, especially in large-scale and complex search spaces. Its principle is based on the physical phenomenon of metal annealing, where a solid is gradually cooled to reduce defects, finding the optimal solution. The process involves heuristic search to compute acceptance probabilities, and by gradually lowering the "temperature," it reduces the probability of accepting larger curve lengths. The high-temperature phase allows for a broad search, while the low-temperature phase converges to the shortest curve length. The steps for controlling the temperature include initialization, iteration, and termination condition determination.

For this problem, this paper determine that if the objective function value changes less than a preset value ($\left|E_{\text{best}} - E_{current}\right| < \varepsilon$) within a certain number of iterations, this paper can consider the algorithm to have converged and stop. Here, ε is a very small positive number representing the precision requirement (1e-5). Additionally, this paper set the temperature threshold to be the radius of the turnaround area plus a very small disturbance value to prevent possible collisions or extreme conditions during the algorithm's execution.

2.5 Bench Dragon Turnaround Path Analysis

Building on section 2.4, this paper further explore the impact of speed adjustment on the normal inward movement of the Bench Dragon. Here, this paper change the speed of the dragon head's front handle under the condition that the speed is fixed and does not exceed 2 m/s, and calculate how the speed change affects the maximum speed of other handles. This paper then solve for the limit of the dragon head's front handle speed under extreme conditions. Under the path setup of section 2.4, no new dragon dance team motion mathematical model needs to be established, and this paper proceed along this path. The dragon head’s speed remains constant, but this paper adjust and test different speeds, recording the speed states of the handle groups in the dragon body after each adjustment and determining if the maximum speed remains below the 2 m/s limit.

3 RESULTS

3.1 Analysis of Experimental Results

Based on the established differential equations, this paper obtained the positional coordinates and velocity magnitudes of the dragon head, the 1st , 51st, 101st, 151st segment at the initial moment, 1s, 50s, 101s, 151s, 201s, and 300s, respectively. Figure 2 illustrate the motion trajectory of the dragon team at the initial time, 1s, 60s, 120s, 180s, 240s, and 300s. As can be seen, even at 300s, all 223 sections of the dragon body have not fully entered the equidistant spiral, and thus, this paper will further explore the termination conditions for the dragon team's continued motion.

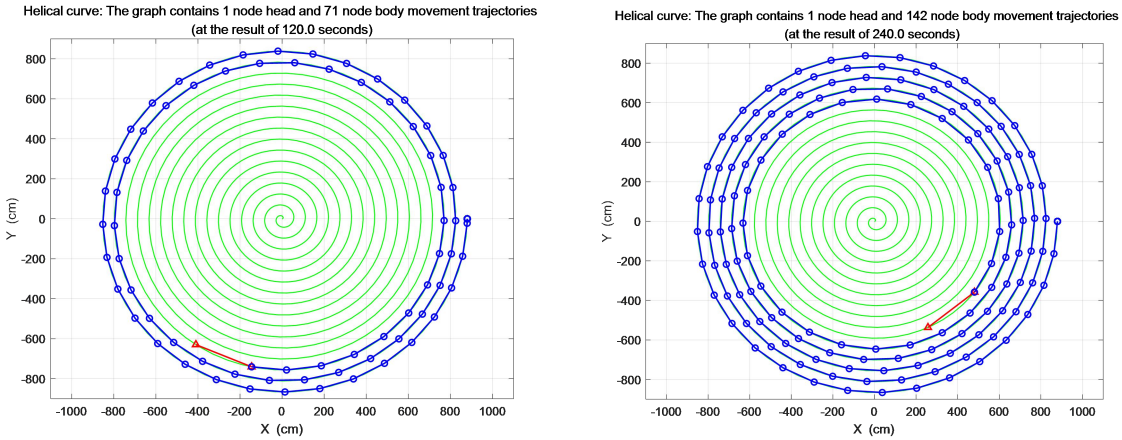

Figure 2 Results of Differential Equation and Recursion-Based Solution

The motion process is simulated with a 0.01s time step, ending at 390.92s, and with a 0.001s step, ending at 391.63s, as per Figure 3 Simulation errors stem from: (1) Time step size, with smaller steps yielding less error due to closer approximation of continuous motion, while larger steps may overlook nuances. (2) Limit condition approximations, where as the spiral's end is reached, error accumulation becomes more pronounced, potentially causing an earlier stopping condition detection with larger time steps. Smaller steps (0.001s) yield more accuracy, while larger steps (0.01s) result in earlier termination due to error build-up.

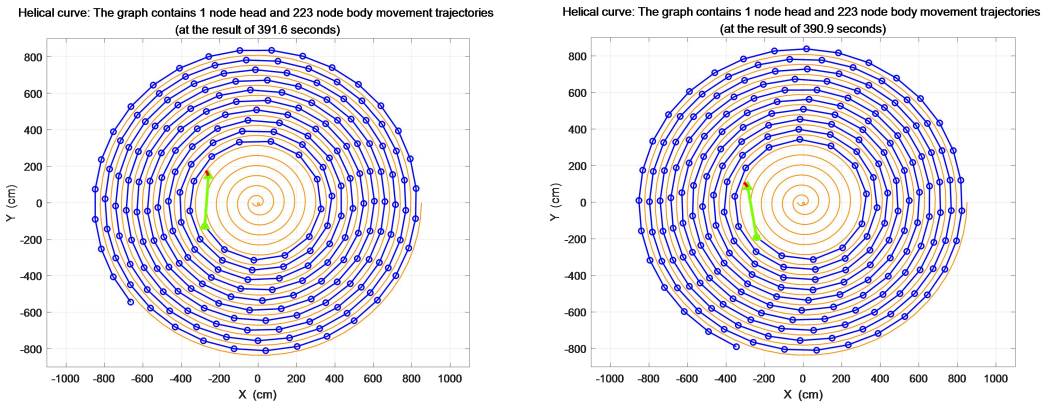

Figure 3 The Final Motion State with a Time Precision of 0.001s (Left Figure) and the Final Motion State with a Time Precision of 0.01s (Right Figure)

The final positions and velocities of the front handles of the 1st, 51st, 101st, 151st, and 201st dragon sections, as well as the rear handles of the dragon's tail, are as follows in Table 1:

Table.1. Position Coordinates of the Bench Dragon

	1st	51st	101st	151st	201st	tail
v(m/s)	0.953593	0.984499	0.990695	0.993352	0.994829	0.995289
x (m)	2.72196	-4.45227	6.008145	7.036571	0.954032	-8.376886
y (m)	-0.313555	-1.517427	0.80352	1.35954	-8.066584	1.496593

Based on the above analysis, it is easy to determine that the minimum pitch satisfying the turning condition lies between 50 cm and 60 cm. Therefore, this paper iterate over the pitch within this range, with a step size of 0.005 cm for each

iteration. The resulting graph of the judgment value (flag) and the time of obstruction termination as a function of pitch size is shown in Figure 4.

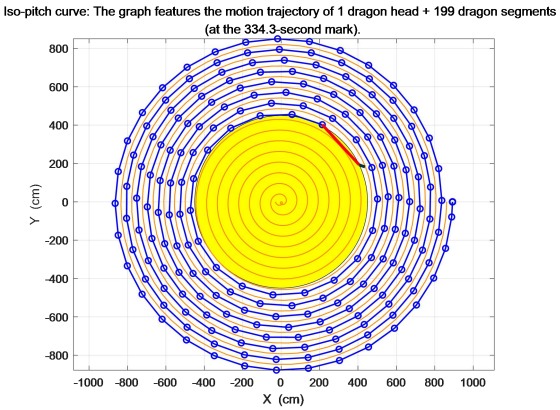

Figure 4 2.3 Experimental Results

In section 2.3, the minimum pitch is 55.758 cm with an obstruction time of 334.34 s. The graph shows the time to encounter obstacles increases slowly from 50cm to 60cm, with a sharp acceleration at 52.8cm, then a gradual decrease to no change. From section 2.2, the pitch value for the dragon head's exact arrival matches where the rate of increase in Figure 4 levels off. For segments other than the head, the front handle's trajectory retraces the bench's path, making the motion of the 223 segments equivalent if time is ignored. If the probability of encountering obstacles is equal for all benches past a certain time, the head has entered the turn-around area, indicating arrival. Thus, the pitch value at the arrival condition change is approximately where the obstacle encounter time rate of increase stops.

In 2.4, the final obtained angle of the longer arc is 3 radians, and the angle of the shorter arc is 2π - 3. Figure 5 shows the turning diagram of the dragon dance team under the optimal solution. Using the method from Section 2.1, the position and velocity changes of each dragon segment from -100s to 100s are calculated. Table.2 and Table.3 are the position and velocity results of the dragon dance team at certain times, along with the corresponding relative positions at the turning points.

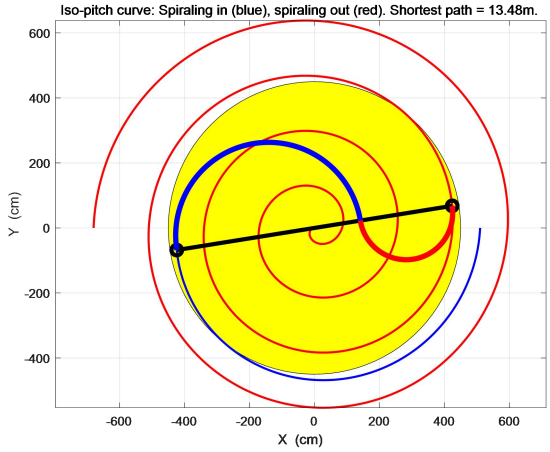

Figure 5 Schematic Diagram of the Entering and Exiting Trajectories

Table 2 Position Results of the Bench Dragon from -100s to 100s.

	-100	-50	0	50	100
head x(m)	8.503941	6.553096	-4.248714	4.076716	0.006748
head y(m)	0.348817	-1.562022	-0.590324	4.644781	8.074771
1st x(m)	7.989437	6.725194	-3.17611	5.628465	2.826317
1st y(m)	3.190113	1.312998	-3.131987	2.223662	7.459531
51st x(m)	10.2	-5.820768	-0.232925	-4.29776	4.235754
51st y(m)	0	-7.632433	-8.063824	-4.421895	0.710841
101st x(m)	10.2	10.2	10.2	-6.064715	-6.324483
101st y(m)	0	0	0	6.813674	4.025013

Table 3 Velosity Results of the Bench Dragon from -100s to 100s

	-100	-50	0	50	100
head (m/s)	1.00000	1.000000	1.000000	1.000000	1.000000
1st (m/s)	0.995391	0.992725	0.982747	0.990664	0.994638
51st (m/s)	0	0.9963	0.994757	0.99101	0.981378
101st (m/s)	0	0	0	0.995902	0.993926
151st (m/s)	0	0	0	0	0.996638

Figure 6 is the result of section 2.5.

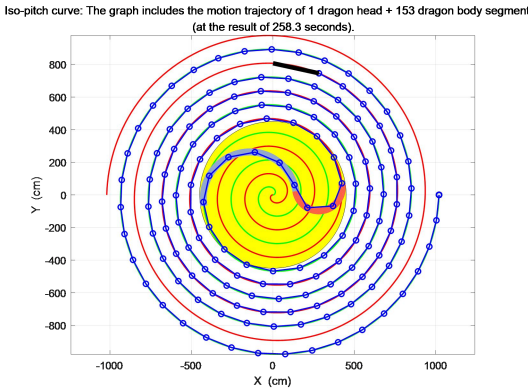

Figure 6 Schematic Diagram of the Entering and Exiting Trajectories

4 CONCLUSIONS

This paper takes the unique folk activity "Bench Dragon" from Zhejiang, Fujian, and other regions as the research subject, exploring its in-and-out motion along an equidistant spiral curve. By establishing a mathematical model, analyzing collision conditions and the turning area, and using the simulated annealing algorithm to solve for the minimum pitch and optimal turning path, the paper ultimately determines the position coordinates, velocity magnitudes, and collision time points at various stages of the Bench Dragon's motion. This paper can obtain these main conclusions: (1) The Bench Dragon is at risk of collision during the entry and exit spiral motion. Due to its leading position and smallest radius, the dragon head is the first to collide. The article calculates the time point of the first collision and determines the minimum pitch required for turning to be 55.758 centimeters; (2) The turning path of the Bench Dragon consists of two S-shaped, tangent semicircles, with one arc having twice the radius of the other. By using an improved simulated annealing algorithm, the article finds the shortest turning path and calculates the position and velocity changes of the dragon head and body during the turning process; (3) The speed variation of the dragon head affects the speed of the dragon body and has a limiting speed. Under the condition that the speed is constant and does not exceed 2 m/s, the article analyzes the impact of speed changes on the maximum speed of other handles and determines the limiting speed of the dragon head. The results of this research provides theoretical support for the study of equidistant spiral motion and contributes to the inheritance and development of traditional folk culture.

COMPETING INTERESTS

The authors have no relevant financial or non-financial interests to disclose.

REFERENCES

[1] Ding Z, Yu Y. Archimedes spiral beam: composite of a helical-axicon generated Bessel beam and a Gaussian beam. JOSA A, 2024, 41(5): 874-880.
[2] Cui W, Deng X, Dong P. Research on Spiral Motion Analysis Based on Optimisation Algorithm and Neural Networks. Academic Journal of Science and Technology, 2024, 13(1): 83-88.
[3] Eppstein D. Locked and unlocked smooth embeddings of surfaces. arxiv preprint arxiv: 2206.12989, 2022.
[4] Yang L, Li Y, Wang Z, et al. Numerical simulation and experimental study on ultrafine powder spiral transportation degassing. Engineering Research Express, 2024, 6(2): 025412.
[5] Apan J J D, Honra J P, Tayo L L. Evaluation of the Effects of Anastomosis Angle on the Performance of an Optimized Spiral Flow-Inducing Graft Design using CFD. CFD Letters, 2023, 15(11): 118-130.
[6] Shuangqing Y U, Guo L I U, Pengyuan Z, et al. A flat-foldable equiangular spiral folding pattern inspired by sunflowers for deployable structures. Chinese Journal of Aeronautics, 2024, 37(6): 425-438.
[7] Wenjian C A O, Dengyong W, Zhiyuan R E N, et al. Evolution of convex structure during counter-rotating electrochemical machining based on kinematic modeling. Chinese Journal of Aeronautics, 2021, 34(3): 39-49.

[8] Greco C, Kotak P, Gallegos J K, et al. Scalable manufacturing system for bionspired twisted spiral artificial muscles (TSAMs). Manufacturing Letters, 2020, 26: 6-11.
[9] Zhu H, Chen J, Ren Z, et al. A new technique for high-fidelity cutting technology for hydrate samples. Journal of Zhejiang University-SCIENCE A, 2022, 23(1): 40-54.
[10] Peterman D J, Hebdon N, Ritterbush K A. Twirling torticones: hydrostatics and hydrodynamics of helically-coiled ammonoids. The American Association of Petroleum Geologists bulletin, 2021.
[11] Liu P, Wu M, Lin G. Optimization Design and Research on Macro Program of Archimedes Spiral Machining//Mechatronics and Automation Technology. IOS Press, 2022: 92-99.
[12] Longardner K, Shen Q, Tang B, et al. An Algorithm for Automated Measurement of Kinetic Tremor Magnitude Using Digital Spiral Drawings. Digital Biomarkers, 2024, 8(1): 140-148.